International Journal of Applied Earth Observation and Geoinformation 135 (2024) 104281

Contents lists available at ScienceDirect

International Journal of Applied Earth Observation and Geoinformation

journal homepage: www.elsevier.com/locate/jag

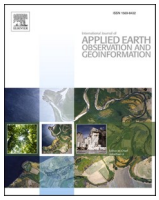

Improved early detection of wheat stripe rust through integration pigments and pigment-related spectral indices quantified from UAV hyperspectral imagery

Anting Guo [a], Wenjiang Huang [a,b,*], Binxiang Qian [a,b], Kun Wang [a,*], Huanjun Liu [c], Kehui Ren [a,b]

[a] Key Laboratory of Remote Sensing and Digital Earth, Aerospace Information Research Institute, Chinese Academy of Sciences, Beijing 100094, China
[b] University of Chinese Academy of Sciences, Beijing 100049, China
[c] State Key Laboratory of Black Soils Conservation and Utilization, Northeast Institute of Geography and Agroecology, Chinese Academy of Sciences, Changchun 130102, China

ARTICLE INFO

Keywords:
Wheat stripe rust
Early detection
UAV hyperspectral images
Pigments
Spectral indices
Radiative transfer model

ABSTRACT

Wheat stripe rust is a significant disease affecting wheat growth, often referred to as the "cancer of wheat". Early and accurate detection of stripe rust is crucial for enabling crop managers to implement effective control measures. Hyperspectral remote sensing methods for crop disease detection have gained significant attention. However, commonly used spectral bands or spectral indices (SIs) from hyperspectral data often fail to capture the subtle changes associated with the early stages of crop diseases accurately. In this study, we propose a method for early detection of wheat stripe rust by combining pigments and SIs retrieved from UAV hyperspectral imagery. We acquired hyperspectral images of wheat stripe rust at 7, 16, and 23 days post-inoculation (DPI) using a UHD 185 hyperspectral sensor (450–950 nm) mounted on an S1000 hexacopter UAV. Pigments, including chlorophylls (Cab), carotenoids (Car), anthocyanins, Cab/Car, and 11 pigment-related SIs, were extracted from UAV hyperspectral images using radiative transfer modeling. The early detection model for wheat stripe rust was developed using these parameters and machine learning algorithms. The results indicated selected pigments and SIs effectively distinguished stripe rust-infected wheat from healthy wheat at 7, 16, and 23 DPI. Models that combine pigments and SIs (PSIMs) perform better than those relying solely on SIs (SIMs) or pigments (PMs). Notably, the RF-based PSIM achieved overall accuracies of 78.1 % and 81.3 % during the asymptomatic (7 DPI) and minimally symptomatic (16 DPI) phases of disease, respectively. Additionally, the pigments in the PSIM contributed more significantly than the SIs, highlighting the importance of pigments in the early detection of stripe rust. Overall, the method combining pigments and spectral indices proposed in this study effectively enhances the early detection of wheat stripe rust and offers valuable insights into the early detection of other crop diseases.

1. Introduction

Global climate change has led to an increase in crop pests and diseases, threatening global food security. Wheat stripe rust, caused by *Puccinia striiformis* (Chen, 2020), is a prevalent disease affecting over 60 countries, including China, the USA, and the UK (Bouvet et al., 2022). Stripe rust can severely reduce wheat yields, with moderate infections typically resulting in a 20–30 % reduction, and severe infections causing losses of over 60 % (Chen et al., 2014). As an airborne disease, stripe rust spores spread easily through wind. Once attached to wheat leaves, they can quickly infect neighboring plants under favorable temperature and humidity conditions (Chen, 2017). Therefore, early and accurate detection of stripe rust, even in the absence of visible symptoms, is crucial for early prevention and control, reducing potential losses for farmers. However, current detection methods, such as visual inspection, field sampling, and laboratory analysis, are often subjective, time-consuming, and labor-intensive, hindering early, accurate, and rapid detection of wheat stripe rust.

Hyperspectral detection techniques have recently emerged as an effective alternative to traditional field surveys for detecting crop

* Corresponding authors.
E-mail addresses: huangwj@aircas.ac.cn (W. Huang), wangk@aircas.ac.cn (K. Wang).

https://doi.org/10.1016/j.jag.2024.104281
Received 23 August 2024; Received in revised form 24 October 2024; Accepted 17 November 2024

diseases. The integration of hyperspectral remote sensing with unmanned aerial vehicles (UAVs) has enabled accurate disease detection at the field scale (Shahi et al., 2023). UAV hyperspectral remote sensing offers fine spectral resolution, effectively capturing changes caused by diseases onset (Moriya et al., 2021). Additionally, UAVs enable frequent, cost-effective detection of small areas, which is crucial for detecting early disease onset and tracking its spread. The general approach to early disease detection with UAV hyperspectral technology involves the direct use of original spectral bands sensitive to the disease, as well as transformed forms such as spectral indices (SIs) (Wu et al., 2023), fractional order differentiation (Zhang et al., 2023), continuum removal (Zhang et al., 2023), and continuous wavelet transforms (Tian et al., 2021). The use of SIs is particularly common, as it highlights disease-related spectral features and reduces background noise and other effects (Marin et al., 2021). Recent studies indicate that crop diseases can be effectively identified by screening sensitive bands and constructing new SIs, and combining them with machine learning algorithms (Tian et al., 2023). Chen et al. (2020) developed new SIs for early identification of peanut blight and confirmed their significant effectiveness in UAV images. Abdulridha et al. (2019) combined multiple SIs with neural networks and discriminant analysis to monitor tomato diseases at various stages, finding that the photochemical vegetation index (PRI) was the most effective. However, SIs have limitations in disease detection, as they rely on only a few bands, providing less detailed information about the disease. This is especially problematic in the early stages of crop disease development, where external features show minimal changes, making accurate detection using spectral information alone particularly challenging.

Using biochemical and biophysical parameters (BPs) within crop leaves for disease detection is a new approach that offers additional disease information beyond spectral features like SIs. when a pathogen infests a crop, complex and variable host-pathogen interaction trigger a range of BPs responses, including changes in pigment content, cellular structure, and water content (Yao et al., 2019). Significant changes in these BPs can occur in the early stages of disease development, even before visible symptoms appear (Rumpf et al., 2010). Wheat stripe rust has been shown to decrease chlorophyll (Cab) content, Nitrogen Balance Index (NBI) and dry matter content while increasing anthocyanin (Anth) content in leaves (Shi et al., 2018). These changes not only underlie spectral variations but can also be directly used for disease detection. For example, Yao et al.(2019) identified early wheat stripe rust-infested leaves by correlating spectra with Cab, finding that this method could detect the disease at least three days before visible symptoms appeared. Most studies have directly monitored diseases using measured BPs. Although effective, these methods cannot be spatially applied, limiting their practical use in early disease detection. Obtaining BPs from UAV and satellite imagery using radiative transfer models (RTMs) can effectively address this issue. RTMs, with their causal and mathematical-physical basis, are robust to changes in geometry, lighting, and background factors, aiding generalization to different environments (Camino et al., 2021). Numerous studies have used RTMs to extract BPs from airborne hyperspectral data for detecting vegetation diseases. For example, Camino et al. (2022) explored detecting *Xylella fastidiosa* (*Xf*)-infected trees using BPs extracted from airborne hyperspectral data. They found that significant changes in maximum carboxylation rate, pigment, carbon-based composition (CBC), and temperature following *Xf* infestation in the trees. Models built on these features achieved over 90 % accuracy in detecting the disease. Zarco-Tejada et al.(2018) achieved pre-symptomatic detection of *Xf* using plant traits quantified from airborne hyperspectral data with a three-dimensional RTM. Later, Zarco-Tejada et al.(2021) also demonstrated, using airborne hyperspectral techniques, the differences between pathogen-induced (*Xf*) subtle physiological changes and the dynamics of abiotic stress (water stress), effectively distinguishing between the two. Poblete et al.(2021) effectively differentiated *Xf*-infected trees from those affected by *Verticillium dahliae* using pigments, chlorophyll fluorescence, the crop water stress index (CWSI), and narrow-band SIs. The aforementioned studies primarily explored the detection of tree diseases using BPs extracted from airborne hyperspectral data. However, the effectiveness of this method in detecting crop diseases, particularly in the early detection of wheat stripe rust, requires further exploration due to the varying effects of different vegetation pathogens on the internal parameters of plant leaves.

UAV hyperspectral remote sensing has gained significant attention for monitoring crop diseases. However, capturing the subtle changes in the early stages (asymptomatic and mild symptom stages) of wheat stripe rust using spectral information alone remains challenging. Crop BPs, particularly pigments, respond rapidly to early disease changes, making them highly promising for early disease monitoring. Therefore, we propose a new method for early detection of wheat stripe rust by combining pigments and SIs. In this study, we collected ground sample data and UAV hyperspectral data during the early stages of wheat stripe rust infestation. Using these data, we will focus on evaluating the effectiveness of combining pigments derived from UAV hyperspectral images with SIs for the early detection of wheat stripe rust. The specific objectives are: (1) to investigate how BPs such as leaf pigments, retrieved through RTM hybrid inversion, change following wheat is infected with the stripe rust pathogen and to assess their ability to distinguish between diseased and healthy wheat; (2) to develop and evaluate an early detection model for wheat stripe rust by integrating pigments and SIs; (3) to evaluate the contribution of pigments and SIs within the early detection model for the disease.

2. Materials and methods

2.1. Study area

The wheat stripe rust experiment was conducted at the Experimental Base of the Chinese Academy of Agricultural Sciences, located in Wanzhuang Town, Guangyang District, Langfang City, Hebei Province, China (39°30′41″N, 116°36′17″E). This region, situated in the North China Plain, primarily cultivates wheat and maize as its main food crops. It experiences a temperate continental monsoon climate, characterized by an average annual temperature of 11.9 °C and annual precipitation of 554.9 mm. Four plots were selected at the experimental site: two designated for stripe rust inoculation and two serving as controls. On 18 April 2018, a suspension of stripe rust fungus spores was sprayed on wheat plots designated for inoculation to induce stripe rust infestation. The inoculation procedure adhered to the guidelines specified in the "Rules for Resistance Evaluation of Wheat to Diseases and Insect Pests Part1: Rule for Resistance Evaluation of Wheat to Stripe Rust" (NY/T 1443.1–2007). Additionally, all plots were managed uniformly throughout the growing period. The locations of the experimental site and plots are shown in Fig. 1A.

2.2. Data acquisition

2.2.1. Ground sample

Three data acquisition experiments were conducted on April 25, May 4, and May 11, 2018, corresponding to 7, 16, and 23 DPI of wheat stripe rust, respectively. Eight 1 × 1 m sampling points were established in each experimental plot to collect ground sample data (Fig. 1C). Sixteen samples were collected from each of healthy and diseased inoculated plots in each experimental campaign, resulting in a total of 32 samples. We examined 40 wheat plants at each sampling site to evaluate disease severity. The disease index (DI) was used to describe the severity of stripe rust at each sampling point. The stripe rust survey method and DI calculation followed the "Rules for Monitoring and Forecasting of Wheat Stripe Rust" (GB/T 15795-2011) (Guo et al., 2021). Our survey of disease severity indicated that the DI at 7 DPI and 16 DPI ranged from approximately 0 to 3, indicating very mild disease, whereas the DI at 23 DPI ranged from approximately 16 to 30, indicating mostly moderate

Fig. 1. Experimental area location and plot distribution. A represents the location of the experimental area; B represents UAV hyperspectral data acquisition activity; C represents UAV hyperspectral image and sample location; D represents the status of healthy and diseased samples at different infestation periods. D1-D3 represent healthy samples, and D4-D6 represent diseased samples at 7, 16, and 23 days post-inoculation (DPI), respectively.

disease (Fig. 1D). Additionally, at each sampling site, we measured Cab, NBI, and Anth using a Dualex instrument (Force-A, Orsay, France), and leaf area index (LAI) using the LAI-2200 plant canopy analyzer (LI-COR, Lincoln, NE, USA).

2.2.2. UAV hyperspectral images

Fig. 1B shows a UAV hyperspectral observation experiment conducted in the wheat stripe rust experimental area. The S1000 hexacopter UAV (SZ DJI Technology Co., Ltd., Guangdong, China) was used for the aerial photography missions. It provides excellent stability and load capacity for extended missions in complex environments, offering the flexibility to integrate multiple cameras and sensors for various applications. A UHD 185 hyperspectral sensor (Cubert GmbH, Ulm, Germany) was mounted on the UAV to acquire hyperspectral images. Its lightweight design makes it ideal for UAVs, enabling real-time data acquisition and processing, supporting precise target identification and analysis. The UHD 185 sensor covers a spectral range of 450–950 nm with a spectral resolution of approximately 4 nm. The UAV flight parameters were as follows: an altitude of 30 m, a speed of 4 m/s, with flight paths having approximately 80 % forward overlap and 60 % lateral overlap. UAV hyperspectral images with a spatial resolution of 1.2 cm were obtained at three different stages following wheat stripe rust infestation. UAV hyperspectral image acquisition was conducted between 11:00 a.m. and 1:00p.m. under clear weather conditions with minimal wind. Photographing the whiteboard before aerial imaging ensures that radiometric corrections will be applied to the UAV hyperspectral data. Hyperspectral data preprocessing was carried out after acquiring the UAV data. First, invalid images were deleted to minimize unnecessary data processing. Next, Radiometric correction was automatically applied using Cubert Utils Touch (Cubert GmbH, Ulm, Germany), obtaining reflectance data for the UAV hyperspectral images (Zhu et al., 2020). Hyperspectral and panchromatic image fusion was also performed using this software. The images were then stitched and exported using Agisoft Photoscan Professional Pro (Agisoft LLC, St. Petersburg, Russia). Finally, the average spectra of corn samples were extracted using regions of interest (ROI) in ENVI 5.6 (Exelis Visual Information Solutions, Boulder, Colorado) (Guo et al., 2021), and spectral noise in the UAV hyperspectral data was removed using the Savitzky-Golay (S-G) smoothing method (Suarez et al., 2021).

2.3. Methods for early detection of wheat stripe rust

A method for the early detection of wheat stripe rust was developed based on ground sample data and UAV hyperspectral data collected during the three infestation stages of the disease. The method comprises three main modules: data preparation, feature extraction and selection for early disease detection, and the construction and evaluation of the detection model (Fig. 2).

2.3.1. Crop BPs for hybrid model inversion

In this study, key features for detecting wheat stripe rust included pigments (Cab, Car, Cab/Car, Anth), LAI, and leaf inclination distribution function (LIDF) extracted from UAV hyperspectral images. Wheat BPs were inverted using a hybrid model that combines the PROSAIL model with the Gaussian process regression (GPR) algorithm. The PROSAIL model integrates the PROSPECT-PRO model at the leaf level with the 4SAIL model at the canopy level (Berger et al., 2020; Guo et al., 2023). Canopy reflectance data at 1 nm intervals across the 400–2500 nm range, along with corresponding parameter data, were simulated using the PROSAIL model based on the input ranges for each parameter listed in Table 1. To align with the UAV hyperspectral sensor settings, the simulated data were resampled to a spectral range of 450–950 nm at 4 nm intervals. The 20,000 sets of spectral data and BPs generated from the simulation were randomly divided into two groups: 70 % for training and 30 % for testing. GPR is a probabilistic, non-parametric regression method widely used in constructing hybrid models for vegetation parameter retrieval (Danner et al., 2021; Estévez et al., 2022). The simulation-generated training samples were input into the GPR algorithm for model training. The coefficient of determination (R^2) and root mean square error (RMSE) were used to evaluate the model's accuracy on the test samples. The trained GPR model was then applied to UAV hyperspectral data to retrieve crop BPs. The inverted BPs were validated using measured sample data for LAI and Cab, as these were the only parameters with available measured data (Poblete et al., 2020; Zarco-Tejada et al., 2021; Longmire et al., 2022). The hybrid model was implemented in the ARTMO toolbox (Automatic Radiative Transfer Modeling Operator) (Verrelst et al., 2015).

2.3.2. Pigment-related spectral indices

To evaluate the effectiveness of SIs and their integration with crop

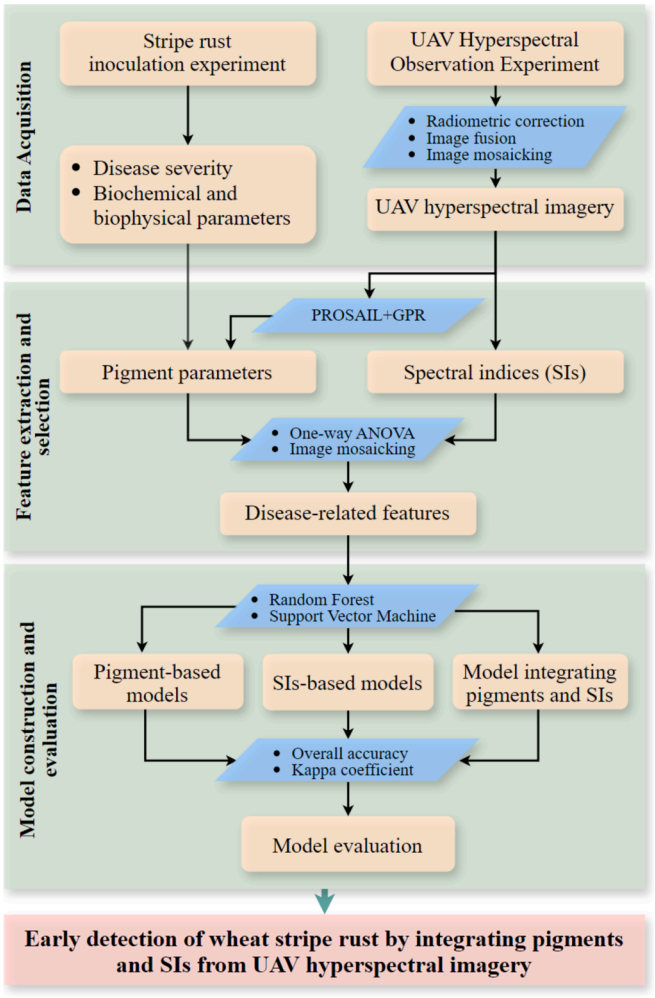

Fig.2. Schematic illustration of the early detection of wheat stripe rust by integrating pigments and SIs from UAV hyperspectral imagery.

Table 1
Range of parameter settings used in PROSAIL for this study.

Model	Parameters	Description	Unit	Range
PROSPECT-PRO	N	Leaf structure	unitless	1.5
	Cab	Leaf chlorophyll content	ug/cm^2	10–70
	Car	Leaf carotenoid content	ug/cm^2	2–20
	Anth	Leaf anthocyanin content	ug/cm^2	0.1–2
	Cw	Leaf water content	cm	0.01
	Cp	Leaf protein content	g/cm^2	0.0010
	Cb	Brown pigment content	ug/cm^2	0
	CBC	Carbon-based constituents	g/cm^2	0.001–0.006
4SAIL	LIDF	Leaf inclination distribution function	deg	20–70
	LAI	Leaf area index	m^2/m^2	0–7
	HOT	Hot spot parameter	m/m	0.01
	SZA	Solar zenith angle	deg	30
	OZA	Observer zenith angle	deg	0
	RAA	Relative azimuth angle	deg	0
	BG	Soil brightness	unitless	0.5

pigments in the early detection of wheat stripe rust, we selected 34 SIs related to pigments such as Cab, Car, Anth, and Cab/Car as potential features for constructing a wheat stripe rust monitoring model. These SIs are listed in Table 2.

Table 2
Alternative SIs used for detecting wheat stripe rust in this study.

SIs	Formula	Reference
Chlorophyll indices		
VOG1	$VOG1 = R_{742}/R_{722}$	(Vogelmann et al., 1993)
VOG2	$VOG2 = (R_{734} - R_{746})/(R_{714} + R_{726})$	
VOG3	$VOG3 = (R_{734} - R_{746})/(R_{714} + R_{722})$	
GM1	R_{750}/R_{550}	(Gamon et al., 2016)
GM2	R_{750}/R_{702}	
MCARI	$((R_{702} - R_{670}) - 0.2(R_{702} - R_{550}))(R_{702}/R_{670})$	(Daughtry et al., 2000)
MCARI1	$1.2[2.5(R_{802} - R_{670}) - 1.3(R_{802} - R_{550})]$	(Haboudane et al., 2004)
MCARI2	$\frac{1.5[2.5(R_{802} - R_{670}) - 1.3(R_{802} - R_{550})]}{\sqrt{(2R_{802}+1)^2 - (6R_{802} - 5\sqrt{R_{670}}) - 0.5}}$	
TCARI	$3((R_{702} - R_{670}) - 0.2(R_{702} - R_{550})(R_{702}/R_{670}))$	(Haboudane et al., 2002)
TCARI/OSAVI	$\frac{3[(R_{702} - R_{670}) - 0.2(R_{702} - R_{550})(R_{702}/R_{670})}{((1+0.16)\cdot(R_{802} - R_{670})/(R_{802} + R_{670} + 0.16))}$	
CIR	$R_{750}/R_{710} - 1$	
CRI550	$(1/R_{510}) - (1/R_{550})$	(Gitelson et al., 2003)
CRI700	$(1/R_{510}) - (1/R_{702})$	
CRI515,550	$(1/R_{514}) - (1/R_{550})$	
CRI515,700	$(1/R_{514}) - (1/R_{702})$	
R_{NIR}*CRI550	$((1/R_{510}) - (1/R_{550}))*R_{770}$	(Gitelson et al., 2006)
R_{NIR}*CRI700	$((1/R_{510}) - (1/R_{702}))*R_{770}$	
PSSRa	R_{802}/R_{674}	(Blackburn, 1998)
PSSRb	R_{802}/R_{650}	
PSSRc	R_{802}/R_{502}	
PRI570	$(R_{570} - R_{530})/(R_{570} + R_{530})$	(Gamon et al., 1992)
PRI515	$(R_{514} - R_{530})/(R_{514} + R_{530})$	(Hernández-Clemente et al., 2011)
PRIm1	$(R_{514} - R_{530})/(R_{514} + R_{530})$	
PRIm2	$(R_{602} - R_{530})/(R_{602} + R_{530})$	(Gamon et al., 1992)
PRIm3	$(R_{670} - R_{530})/(R_{670} + R_{530})$	
PRIm4	$(R_{570} - R_{530} - R_{670})/(R_{570} + R_{530} + R_{670})$	(Hernández-Clemente et al., 2011)
PRIn	$PRI_{570}/[RDVI\cdot(R_{702}/R_{670})$	(Calderón et al., 2013)
PRI*CI	$(R_{570} - R_{530})/(R_{570} + R_{530})\cdot((R_{762}/R_{702}) - 1)$	(Garrity et al., 2011)
Anthocyanin indices		
ARI	$1/R_{550} - 1/R_{702}$	(Gitelson et al., 2001)
Carotenoid indices		
SIPI1	$(R_{802} - R_{450})/(R_{802} - R_{680})$	(Penuelas et al., 1995)
SIPI2	$(R_{802} - R_{505})/(R_{802} - R_{690})$	
PSRI	$(R_{682} - R_{502})/R_{750}$	(Merzlyak et al., 1999)
PSNDc	$(R_{802} - R_{502})/(R_{802} + (R_{502})$	(Blackburn, 1998)
Chlorophyll/Carotenoid indices		
CCI	$(R_{530} - R_{646})/(R_{530} + R_{646})$	(Gamon et al., 2016)

2.3.3. Selection of BPs and spectral indices

To develop an effective and concise model for the early detection of wheat stripe rust, a feature selection analysis of candidate SIs and BPs was performed. First, SIs and BPs obtained during the three periods following disease inoculation were evaluated using one-way analysis of variance (ANOVA) (De Castro et al., 2015). Standardized ANOVA is a commonly used statistical method for comparing the means of multiple independent groups to assess statistical significance (Trifi et al., 2022). In this method, the study population is divided into groups based on a single factor (e.g., healthy and diseased wheat), with the dependent variable typically being a continuous numerical variable (e.g., pigments or SIs). One-way ANOVA assesses whether the means differ significantly between groups by comparing between-group variance with within-group variance and calculating the P-value from the F-statistic. Generally, a P-value less than 0.05 indicates a significant difference between healthy and diseased wheat. Features showing significant differences (P

< 0.05) between healthy and diseased samples across all three periods were retained. Next, multicollinearity among the features selected by one-way ANOVA was assessed using Variance Inflation Factor (VIF) analysis to ensure minimal covariance, thereby enhancing the model's accuracy and efficiency. Multicollinearity is considered minimal when variables have VIF ≤ 10 (Tian et al., 2021). Ultimately, the SIs and BPs identified through these two feature selection processes were used to build a model for the early detection of wheat stripe rust. This study conducted one-way ANOVA and VIF analysis following the procedures outlined in Statistical Products and Services Solutions (SPSS 27, IBM Corporation, Armonk, NY, USA).

2.3.4. Construction and evaluation of wheat stripe rust early detection model

In this study, we developed three models for the early detection of wheat stripe rust, based on selected SIs and pigments. These models include one based on SIs (SIM), one based on crop pigments (PM), and one integrating crop pigments and SIs (PSIM). The PSIM was primarily designed to evaluate whether integrating of SIs and crop pigments could enhance the early detection of wheat stripe rust. The first two models were primarily designed to evaluate the effectiveness of using either pigment-related SIs or pigments alone for early detection of wheat stripe rust. These models also served as controls for the PSIM. The three models are constructed using Random Forest (RF) and Support Vector Machine (SVM) algorithms. RF is a powerful ensemble learning method that constructs multiple decision trees during training and outputs class predictions for each. Each tree is built using a random subset of the training data and features to ensure diversity. This randomness helps reduce overfitting and improves generalization performance (Breiman, 2001). SVM is a binary classifier that constructs a separating hyperplane to maximize the margin between positive and negative samples in feature space. The key to class separation lies in using a kernel function to map vectors to a high-dimensional space (Gu et al., 2019). In this study, the Radial Basis Function (RBF), known for its efficiency, was selected to train the model (Camino et al., 2022). Additionally, Bayesian optimization, which uses a Gaussian process, efficiently utilizes prior information, requires fewer iterations, and operates at a faster speed (Snoek et al., 2012). It has also been increasingly used for tuning parameters in models for vegetation disease monitoring (Zarco-Tejada et al., 2021; Poblete et al., 2023). Therefore, Bayesian optimization methods were used to select hyperparameters (including the number of trees, random predictors, and maximum tree depth) in Random Forests, as well as key parameters (cost and gamma) in SVM. Due to the small sample size in each period, the leave-one-out cross-validation (LOOCV) method was employed to train and validate the data. LOOCV excludes one sample from the dataset for validation and uses the remaining samples for training. This method maximizes data utilization and improves the effectiveness of the trained model, especially when the dataset is small (Maimaitijiang et al., 2019). Overall accuracy (OA) and Kappa coefficient were used as the model's accuracy evaluation indices. Additionally, feature importance was assessed using the permutation importance method (Breiman, 2001) to analyze the contribution of each feature (SIs and pigments) in the wheat stripe rust detection model. The permutation importance method works by randomly shuffling the values of a feature and recalculating the model's performance using the shuffled data. The difference between the model's shuffled performance and its baseline performance is then compared; the greater the performance decreases, the more important the feature is to the model. This process is repeated for each feature, and the effect of each feature on the model's performance is recorded. Finally, the features are ranked by importance according to the magnitude of performance degradation (Breiman, 2001; Wei et al., 2015; Fisher et al., 2019). The above process was carried out using the MATLAB Statistics and Machine Learning Toolbox.

3. Results

3.1. Capacity of crop BPs and SIs to distinguish wheat stripe rust

3.1.1. Measured crop BPs

Fig. 3 illustrates the differences in Cab, Anth, NBI, and LAI between healthy and diseased samples, along with their changes as the disease progresses. The results indicate that Cab, NBI, and LAI were significantly lower in stripe rust-infected samples, while Anth values were significantly higher than in healthy samples. For instance, at 7, 16, and 23 DPI, the mean Cab values of healthy samples were 23.2, 25.4, and 26.9, while those of diseased samples were 22.9, 24.1, and 24.6. The mean Anth values for healthy samples were 0.045, 0.046, and 0.041, compared to 0.046, 0.059, and 0.078 for infected samples. The differences in Cab and Anth between healthy and infected samples increased over time. For example, the differences in Cab between healthy and diseased samples were 0.3, 1.3, and 2.3 at 7, 16, and 23 DPI, respectively.

3.1.2. Crop BPs retrieved from UAV hyperspectral images using a hybrid model

The hybrid models for crop BPs inversion showed strong performance in the simulated data, with R^2 values above 0.90 for all parameters except Cab/Car (Table 3). The hybrid model was also used to retrieve crop parameters from UAV hyperspectral data, validated against measured LAI and Cab. The results showed that the R^2 values for Cab across the three periods were 0.558, 0.788, and 0.653, with RMSEs of 1.219, 1.519, and 1.543, respectively (Fig. 4). For LAI, the R^2 values were 0.449, 0.603, and 0.42, with RMSEs of 0.311, 0.388, and 0.419, respectively (Fig. 5). These results provide a strong foundation for detecting wheat stripe rust through the retrieved crop BPs.

The ability of crop BPs extracted from hyperspectral data to differentiate between diseased and healthy wheat was assessed using one-way ANOVA. The results showed that pigments (Cab, Car, Cab/Car, and Anth) were significantly different ($P < 0.05$) between healthy and diseased samples across all three infestation periods. The structural parameters (LAI and LIDF) did not show significant differences ($P > 0.05$) between the two groups (Table 4), suggesting that these parameters may not be suitable for early disease detection. Fig. 6 also visualizes

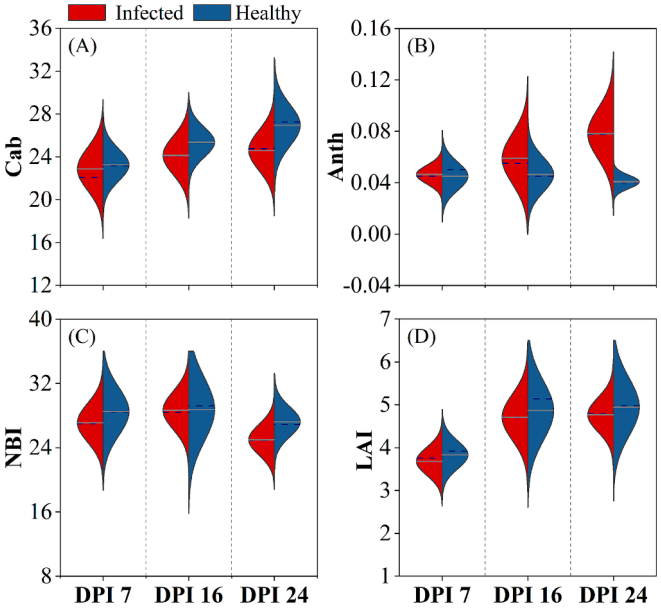

Fig. 3. Differences in measured crop BPs between healthy and diseased samples and their changes with disease progression. A-D corresponds to chlorophyll (Cab), anthocyanin (Anth), nitrogen balance index (NBI), and leaf area index (LAI), respectively. DPI = days post-inoculation.

Table 3
Accuracy of hybrid models for crop BPs inversion in simulated data. Cab = chlorophyll, Car = carotenoid, Anth = anthocyanin, LAI = leaf area index, LIDF = leaf inclination distribution function, R^2 = coefficient of determination, RMSE = root mean square error.

BPs	R^2	RMSE
Cab	0.97	2.67 μg/cm^2
Car	0.92	1.23 μg/cm^2
Anth	0.93	0.58 μg/cm^2
Cab/Car	0.87	1.18
LAI	0.97	0.17 m^2/m^2
LIDF	0.91	5.31°

the differences in each BP between diseased and healthy wheat across the three periods and their variation as the disease infestation progresses. Cab, Car, and Cab/Car were significantly lower in stripe-rusted wheat compared to healthy wheat, while Anth levels were higher. Additionally, the differences between the two groups became more pronounced as the disease infestation progressed. We also conducted a VIF analysis on the crop pigments that showed significant differences in each period. The VIF for each period was less than 5, indicating low covariance among the pigments, confirming their suitability for constructing disease detection models.

3.1.3. Spectral indices

In addition to crop BPs, we evaluated the ability of SIs to distinguish wheat stripe rust using one-way ANOVA. The results showed that 11 SIs were effective ($P < 0.05$) in distinguishing diseased from healthy samples across all three periods. These indices included GM1, GM2, CI, PSRI, PSSRa, PSSRb, PSSRc, PSNDc, PRIm2, PRIm3, CCI, and CIR. Fig. 7 illustrates the differences and variations of representative SIs between diseased and healthy wheat during the three disease infestation periods. The result indicates that PRIm2 in diseased wheat samples showed an increasing trend, while PSNDc, CIR, and GM1 exhibited decreasing trends compared to healthy wheat. The differences between the two became more pronounced as the disease progressed. To build a concise and effective stripe rust detection model, we excluded SIs with high covariance in each period and retained only those with a VIF < 10 (Table 5).

3.2. Performance of different features-based models in detecting wheat stripe rust

We constructed three wheat stripe rust detection models (SIM, PM,

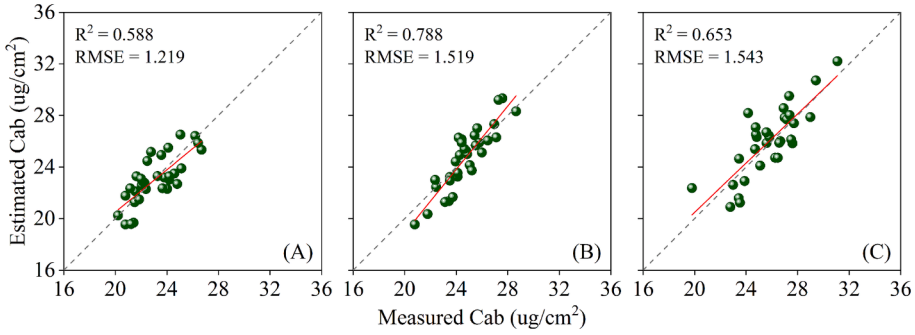

Fig. 4. Validation results for chlorophyll (Cab) inversion using the hybrid model. A-C show the validation results at 7 DPI, 16 DPI, and 23 DPI, respectively. R^2 = coefficient of determination, RMSE = root mean square error.

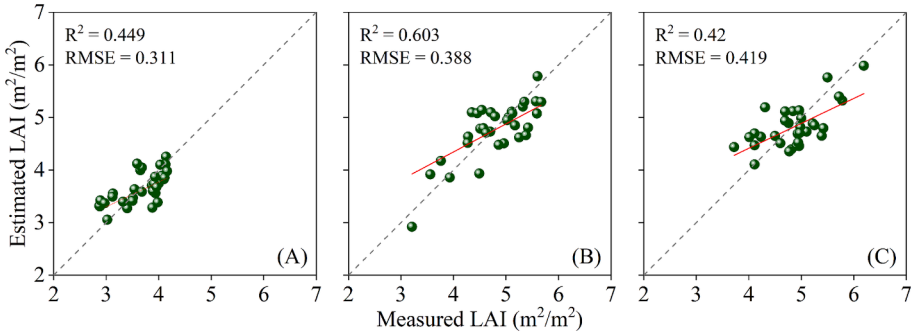

Fig. 5. Validation results for leaf area index (LAI) inversion using the hybrid model. A-C show the validation results at 7 DPI, 16 DPI, and 23 DPI, respectively. R^2 = coefficient of determination, RMSE = root mean square error.

Table 4
One-way ANOVA and VIF tests for inverted crop BPs. DPI = days post-inoculation, P = p-value, VIF = variance inflation factor, Cab = chlorophyll, Car = carotenoid, Anth = anthocyanin, LAI = leaf area index, LIDF = leaf inclination distribution function.

DPI	Methods	Cab	Car	Cab/Car	Anth	LAI	LIDF
7 DPI	P	0.0432	0.037	0.0166	0.0346	0.528	0.219
	VIF	1.21	1.63	1.80	1.32		
16 DPI	P	0.0304	0.0033	0.0026	0.0079	0.4847	0.4087
	VIF	1.86	1.32	1.49	1.62		
23 DPI	P	0.0022	0.0453	6.34E-7	0.0188	0.0521	0.0699
	VIF	2.26	1.51	2.67	1.26		

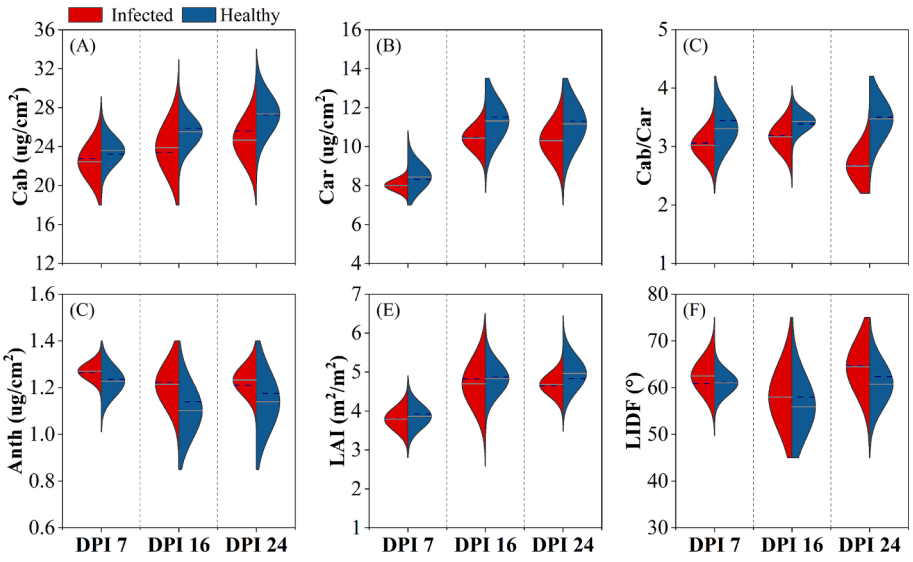

Fig. 6. Differences in retrieved crop BPs between healthy and diseased samples and their changes with the progression of disease infestation. A-F corresponds to chlorophyll (Cab), carotenoid (Car), Cab/Car, anthocyanin (Anth), leaf area index (LAI), and leaf inclination distribution function (LIDF), respectively. DPI = days post-inoculation.

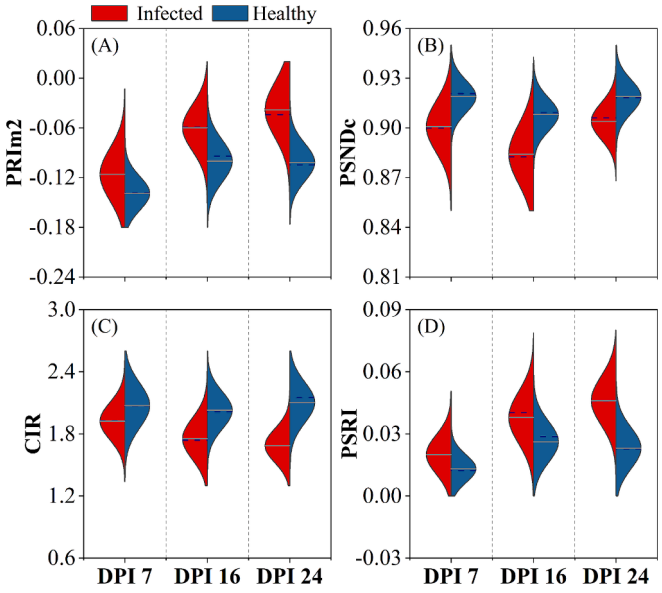

Fig. 7. Differences in SIs between healthy and diseased samples and their changes with the progression of disease infestation. A-D corresponds to PRIm2, PSNDc, CIR and PSRI. DPI = days post-inoculation.

Table 5
SIs selected for each period and their VIF test results. DPI = days post-inoculation, VIF = variance inflation factor.

DPI	Selected SIs and VIF values					
7 DPI	GM1	CIR	PSRI	PSSRc	PSNDc	PRIm2
	7.687	6.110	5.578	8.418	5.023	3.726
16 DPI	CIR	PSRI	PSNDc	PRIm2		
	4.609	5.573	2.567	4.293		
23 DPI	CIR	PSRI	PSSRc	PSNDc	PRIm2	
	6.936	7.262	4.076	3.056	3.131	

and PSIM) using RF and SVM algorithms. Fig. 8 and Table S1 shows the results of wheat stripe rust detection models based on different features. The result shows that the SIM had the lowest performance across all three disease infestation periods, particularly in the early stages (7 DPI and 16 DPI). For example, the RF-based SIM achieved an OA of only 62.5 % and 68.8 %, with kappa values of 0.25 and 0.38 during these two periods. The PM produced acceptable results, with higher accuracy than the SIM across all three disease infestation periods. For example, the accuracy of the RF-based PM exceeded 70 % at 7 DPI and 16 DPI, reaching 84.4 % at 23 DPI. These results highlight the potential of pigments for wheat stripe rust detection. Notably, the PSIM outperformed both SIM and PM in all three disease infestation periods. Specifically, the RF-based PSIM achieved an OA of 78.1 %, 81.3 %, and 87.5 %, with corresponding kappa values of 0.56, 0.63, and 0.75. These results were 6.2 %, 3.2 %, and 3.1 % higher in OA, and 0.12, 0.06, and 0.07 higher in Kappa, compared to the RF-based PM. Furthermore, the OA was 12.5 %, 9.4 %, and 6.2 % higher, and Kappa values were 0.25, 0.19, and 0.12 higher, compared to the RF-based SIM. The superiority of the PSIM over the other two models was more pronounced in the early stages of the disease than in the middle stage. For instance, the RF-based PSIM improved by 12.5 % over the SIM at 7 DPI, compared to a 6.2 % improvement at 23 DPI. Additionally, we observed that the accuracy of all three models increased as the disease progressed. The accuracy of the SVM-based PM was 68.8 % (OA) and 0.38 (kappa) at 7 DPI, increased to 75 % (OA) and 0.5 (kappa) at 16 DPI, and reached 81.3 % (OA) and 0.63 (kappa) at 23 DPI.

3.3. Contribution of pigments and SIs in wheat stripe rust detection

To assess the importance of each pigment and SI in detecting wheat stripe rust, we used the permutation importance method to evaluate feature importance in the SVM- and RF-based PSIM (Fig. 9). Overall, while the importance of each parameter varied across classifiers and periods, the results showed that most pigments received higher importance scores than SIs. Cab, Car, and Cab/Car had higher importance rankings in both SVM- and RF-based PSIMs during the early periods of disease infestation (7 DPI and 16 DPI), while PSNDc ranked higher in the RF-based PSIM. At mid-infestation (23 DPI), Cab/Car and Cab held the top two importance rankings, with CI ranking third. Notably, Cab/Car consistently ranked highest across all periods, indicating that including this indicator in the wheat stripe rust detection model is highly effective. The importance of Anth ranked moderately across all three periods.

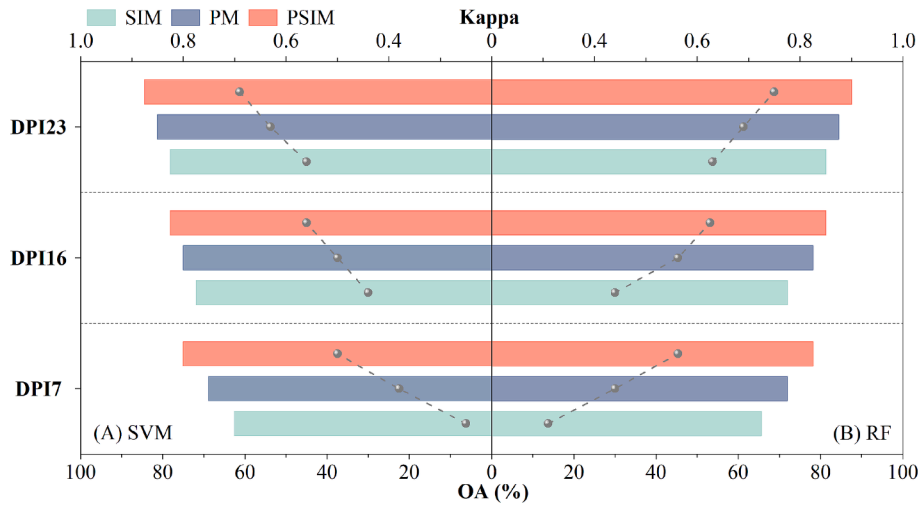

Fig. 8. Accuracy of wheat stripe rust detection models based on different features. A and B represent models constructed with the random forest (RF) and support vector machine (SVM) algorithms, respectively. SIM = the model based on spectral indices, PM = the model based on pigments, PSIM = the model integrating crop pigments and spectral indices, OA = Overall accuracy, Kappa = Kappa coefficient, DPI = days post-inoculation.

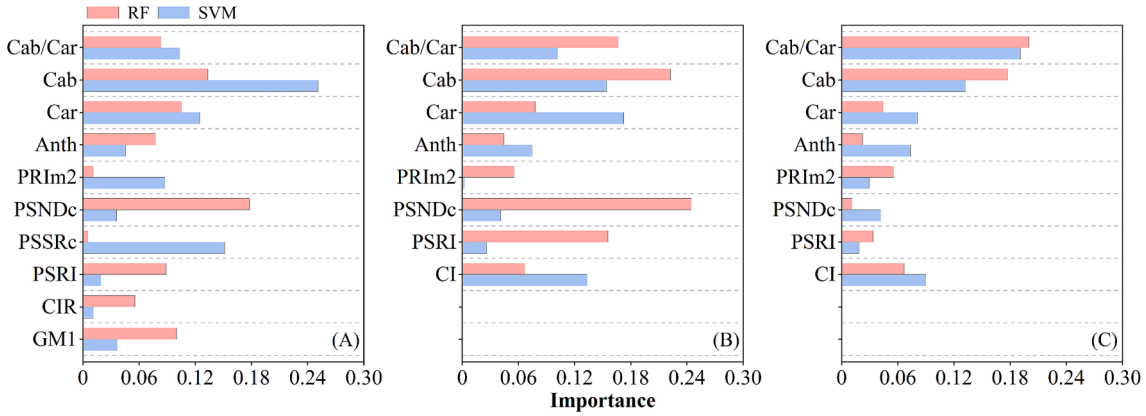

Fig. 9. Importance of crop pigments and SIs in wheat stripe rust detection at (A) 7 DPI, (B) 16 DPI, and (C) 23 DPI. RF = the model based on random forest algorithm, SVM = the model based on support vector machine, Cab = chlorophyll, Car = carotenoid, Cab/Car, Anth = anthocyanin.

4. Discussion

4.1. Pigments and SIs for detecting wheat stripe rust

This study proposes monitoring wheat stripe rust using crop pigments and SIs extracted from UAV hyperspectral data. To verify the effectiveness of crop BPs in distinguishing stripe rust-infected wheat from healthy wheat, we first analyzed measured parameters. We observed decreases in Cab, NBI, and LAI in stripe rust-infected wheat, alongside a significant increase in Anth, consistent with the findings of Camino et al. (2021). Variations in measured BPs between healthy and diseased samples form the basis for detecting wheat stripe rust using BPs derived from UAV hyperspectral data. The results showed that trends in Cab, Anth, and LAI obtained from model inversion aligned with changes observed in measured data for these BPs. Additionally, Car and Cab/Car decreased following disease infestation. Furthermore, one-way ANOVA revealed significant differences in the four pigments (Cab, Anth, Car, and Cab/Car) between healthy and diseased samples across all three infestation periods. Notably, these differences were detectable as early as 7 DPI, highlighting the feasibility of early detection for wheat stripe rust.

Changes in these crop BPs may be linked to plant defense mechanisms and the impact of pathogenic bacteria on plant cells. Notably, Anth, a secondary metabolite with antioxidant properties, increase in response to oxidative stress induced by pathogenic bacterial infestation. This increase enables the scavenging of reactive oxygen species (ROS), thereby mitigating oxidative damage (Clemente et al., 2021). Stripe rust fungus damages plant cell structures, including chloroplasts, inhibiting the synthesis of Cab and Car. This reduction in pigment levels impedes photosynthesis, a process critical for crop growth. Furthermore, since Cab and Car are crucial for photosynthesis, a reduction in their levels inhibits this process in crops. This study is the first to propose Cab/Car as a detection indicator for stripe rust. Typically, this ratio remains stable in healthy vegetation, around 3:1 (Gamon et al., 2016). Our results indicated that wheat infested with stripe rust exhibited a decrease in Cab/Car. This decrease is primarily due to the disease reducing both Cab and Car content, with Cab levels declining more rapidly than Car levels, consistent with Watt et al.(2023). Additionally, the results showed that Cab/Car had high importance scores in the model across different infestation periods, likely because Cab/Car is unaffected by vegetation type, species, or growth period. We also found that changes in LAI and LIDF were minimal across all three periods after wheat disease infestation, making it difficult to distinguish diseased wheat from healthy wheat. This is primarily because, in the early and middle stages of infestation, the disease causes less severe damage, affecting internal leaf BPs more than external morphological characteristics. If the disease progresses to a later stage, it may lead to a reduction in LAI. Watt et al. (2023) found that LAI contributed more significantly in the later stages

of the disease when detecting radiata pine wilt.

The study's results indicated that GM1, GM2, CIR, PSSRa, PSRI, and PSNDc, associated with Cab and Car, tended to decrease following disease infestation in wheat, possibly due to reduced levels of Cab or Car. PRIm2 and PRIm3 are extensions of PRI, closely related to plant light energy use efficiency, and are typically inversely related to each other. Their increase after disease infestation is primarily due to disease reducing light energy use efficiency in crops, resulting in a higher PRI (Hernández-Clemente et al., 2019). The CCI was strongly correlated with Cab/Car, and a decrease in CCI was associated with a decrease in Cab/Car. We found that the Anth-related SI (ARI) passed the test at 7 DPI but not at 16 or 23 DPI. This is likely because ARI is influenced by background, vegetation structure, and other factors, leading to unstable variability between healthy and diseased samples at different infestation stages. Another reason could be ARI's limited capacity for disease differentiation. This aligns with our results, where Anth exhibited moderate feature importance in the model across disease infestation stages.

4.2. Wheat stripe rust detection models based on different features

We explored the use of SIs, pigments, and their combination to construct a wheat stripe rust detection model. While SI-based methods are commonly used for disease detection, this study found they performed the worst across all three disease infestation periods compared to other methods. This may be because SIs, derived from several spectral bands, reflect less specific information about the disease. Additionally, the SIs used were generic and not specifically designed for detecting stripe rust. Although they met the selection criteria, the spectral bands used may not effectively capture information specific to wheat stripe rust. Better results may be achieved with SIs specifically designed for wheat stripe rust, as demonstrated by Zheng et al. (2018), who developed a Sentinel 2 satellite-based SI for stripe rust detection. In this study, the PM demonstrated acceptable performance. Generally, disease detection using measured BPs is more accurate, but these BPs are typically point data, which limits their spatial application. In contrast, models constructed from BPs extracted from UAV hyperspectral images can be spatially extended, offering a practical solution. Previous studies have also shown good performance with models using simulated BPs (Camino et al., 2022; Poblete et al., 2023).

The PSIM achieved optimal detection results, particularly during the early infestation stages (7 and 16 DPI), with accuracies of 78.1 % and 81.3 %, respectively. This provides a methodological basis for early and accurate detection of stripe rust. The model's optimal performance may be attributed to the mildness of the disease in its early stages, requiring more effective features to accurately capture disease information. The combination of crop pigments and SIs captures both internal pigments changes in wheat leaves and the spectral response to the disease. Previous studies have shown that combining SIs and pigments yields better disease detection results in forest trees (Zarco-Tejada et al., 2018; Watt et al., 2023). Our study confirms, for the first time, that this method is also highly effective in the early detection of wheat stripe rust. Additionally, we observed that the performance of the PSIM improved as the infestation progressed. Specifically, the OA of the RF-based PSIM model was 75 %, 78.1 %, and 87.5 %, with Kappa values of 0.50, 0.56, and 0.75 at 7, 16, and 23 DPI, respectively. This improvement may be attributed to the varying sensitivities of the features used in the model at different stages of infestation. During the early stages of infestation (7 and 16 DPI), the disease is less severe and causes minimal disruption to the leaf's internal cellular structure, resulting in smaller changes in pigments and spectral reflectance. By the middle stage of infestation (23 DPI), the disease becomes more severe, causing greater damage to the leaf's internal structure, leading to significant pigment changes. Additionally, the yellow spores attached to the leaf at this stage further impact the spectral data. These observations are consistent with findings from previous studies on vegetation disease monitoring (Gu et al., 2019; Guo et al., 2021). The practical value of our proposed PISM is demonstrated by its ability to be directly applied to UAV hyperspectral imagery of wheat fields, generating farm-scale distribution maps of early disease occurrence. Using these disease distribution maps, agricultural managers can apply targeted treatments to prevent further disease spread, thereby reducing yield losses.

Assessing feature importance in PSIM aids in understanding the contributions of crop pigments and spectral indices to the model. The study results indicate that the feature importance scores for Cab, Car, and Cab/Car are generally higher than those for the SIs in both SVM and RF models, underscoring the significant role of pigment in the models. However, we observed differences in feature importance ratings between the SVM and RF models. This discrepancy may arise from the distinct mechanisms employed by the SVM and RF algorithms in data processing: SVM focuses on identifying decision boundaries, whereas RF makes predictions through the integration of multiple decision trees (Hearst et al., 1998; Breiman, 2001). This intrinsic difference can result in the same features exhibiting significant variations in importance between the two models. Additionally, correlations between features may lead to overestimation or underestimation in one model. Feature importance has also been shown to vary across different algorithmic models in studies by Camino et al.(2022).

4.3. Challenges and prospects

We primarily selected pigments to construct the wheat stripe rust detection model. Although BPs like Cp and Cw have been utilized in other studies, we did not consider them here due to the spectral range limitations of the UAV hyperspectral sensor, which restricts their inversion in the hybrid model. Specifically, the optimal spectral range for estimating Cp is 1500–1700 nm (Féret et al., 2021), while Cw is significantly correlated with bands in the 1000–1700 nm range. However, our UAV hyperspectral sensor captures spectral information only in the 450–950 nm range. When using crop BPs from RTM inversions, uncertainty in the physical model inversion can affect the performance of the hybrid model. We mitigated the RTM inversion uncertainty by restricting parameters in the PROSAIL model to practical ranges, thereby eliminating unexpected parameter combinations. Although flight parameters were consistent across all three missions, human errors during UAV hyperspectral imaging could impact image quality, potentially affecting the accuracy of wheat stripe rust detection. Model uncertainty affects reliability and generalizability. To enhance the performance of wheat stripe rust detection models and reduce uncertainty, we concentrated on machine learning algorithm selection, hyperparameter optimization, and feature selection. However, the experimental data for this study were collected from a single location and specific disease inoculation experiments, which may limit the model's generalizability and increase uncertainty. In future studies, we will gather data on naturally occurring wheat stripe rust across various regions, wheat varieties, soil types, and climatic conditions, alongside simulated data generated by methods such as bootstrapping (Gasmi et al., 2022). This data will be used in combination to validate the model's generalizability and robustness, as well as to analyze model uncertainty, thereby enhancing our understanding of model performance. The model was developed using LOOCV instead of the traditional train-test split method. This approach includes test data in parameter tuning, potentially impacting the model's generalization capability. In the future, we intend to expand the dataset and employ independent datasets for parameter tuning to enhance the model's generalization ability.

In this study, we conducted early detection of wheat stripe rust using SIs extracted from UAV hyperspectral data and pigments. Besides BPs and spectral features, Solar-induced fluorescence (SIF) has garnered increased attention in vegetation disease monitoring for its capacity to detect fine-scale changes in crop photosynthetic physiology induced by disease (Berger et al., 2022; Wu et al., 2022). Currently, most studies focus on disease identification using ground-based SIF sensors, with

limited research on UAV-mounted SIF sensors for disease monitoring (Du et al., 2023). In the future, we aim to utilize UAV-mounted sensors that can acquire SIF alongside hyperspectral sensors to enhance early monitoring of wheat stripe rust. Additionally, SIF data can be simulated using the SCOPE model (Belwalkar et al., 2022; Wu et al., 2024), warranting further investigation into the performance of early monitoring of stripe rust using simulated SIF data. Moreover, UAV thermal imaging data have proven significant in detecting other vegetation diseases (Poblete et al., 2021; Camino et al., 2022). Future studies will investigate whether integrating thermal data, SIF, hyperspectral data, and BPs can improve early detection of wheat stripe rust. Monitoring disease occurrence over large areas and extended time periods can be achieved through satellite, offering valuable decision support to managers. In future studies, we aim to extend the combined pigment and SIs method for early detection of wheat stripe rust to the hyperspectral satellite. However, applying this method using satellite hyperspectral data presents certain limitations. Specifically, satellite hyperspectral data are influenced by atmospheric scattering and absorption during acquisition, necessitating complex atmospheric corrections that can introduce errors. Additionally, the spatial resolution of satellite hyperspectral images is relatively low, resulting in mixed pixel phenomena. This can potentially reduce the accuracy of crop disease detection. Deep learning methods hold great promise for crop disease monitoring, with some studies already demonstrating their effectiveness and offering new perspectives (Deng et al., 2023; Tang et al., 2023; Tasci et al., 2023; Liu et al., 2024). We plan to incorporate deep learning into our proposed method to enhance the accuracy of wheat stripe rust monitoring.

5. Conclusion

This study proposes a method to fuse pigments and SIs extracted from UAV hyperspectral images for the early detection of wheat stripe rust. Results indicated that pigments (Anth, Cab, Car, and Cab/Car) retrieved from UAV hyperspectral data using a hybrid model effectively differentiated between healthy wheat and those early-infested with stripe rust ($P < 0.05$). Three models for detecting wheat stripe rust-SIM, PM, and PSIM-constructed using machine learning algorithms (RF and SVM), demonstrated that PSIM achieved optimal performance during the three periods of disease infestation. The OA of the RF-based PSIM reached 78.1 %, 81.3 %, and 87.5 % at 7, 16, and 23 DPI, respectively. Notably, this model's advantage over the other two is more pronounced in the early stages. This advantage is likely due to the model's ability to capture richer pigments and spectral changes associated with the early stages of the disease. Overall, this study demonstrates that combining crop pigments and SIs extracted from UAV hyperspectral images effectively improves the early detection accuracy of wheat stripe rust. This research advances the early detection of wheat stripe rust and establishes a foundation for detecting other crop diseases.

CRediT authorship contribution statement

Anting Guo: Writing – review & editing, Writing – original draft, Visualization, Validation, Methodology, Investigation, Formal analysis, Conceptualization. **Wenjiang Huang:** Writing – review & editing, Supervision, Funding acquisition, Formal analysis. **Binxiang Qian:** Software, Investigation, Formal analysis, Data curation. **Kun Wang:** Resources, Investigation. **Huanjun Liu:** Validation, Software, Data curation. **Kehui Ren:** Software, Investigation, Formal analysis.

Declaration of competing interest

The authors declare that they have no known competing financial interests or personal relationships that could have appeared to influence the work reported in this paper.

Acknowledgments

This article was supported by the National Key R&D Program of China (2023YFB3906203).

Appendix A. Supplementary material

Supplementary data to this article can be found online at https://doi.org/10.1016/j.jag.2024.104281.

Data availability

Data will be made available on request.

References

Abdulridha, J., Ampatzidis, Y., Kakarla, S.C., Roberts, P., 2019. Detection of target spot and bacterial spot diseases in tomato using UAV-based and benchtop-based hyperspectral imaging techniques. Precis. Agric. [J] 21, 955–978.
Belwalkar, A., Poblete, T., Longmire, A., Hornero, A., Hernández-Clemente, R., Zarco-Tejada, P.J., 2022. Evaluation of SIF retrievals from narrow-band and sub-nanometer airborne hyperspectral imagers flown in tandem: Modelling and validation in the context of plant phenotyping. Remote Sens. Environ. 273, 112986.
Berger, K., Verrelst, J., Féret, J.-B., Hank, T., Wocher, M., Mauser, W., Camps-Valls, G., 2020. Retrieval of aboveground crop nitrogen content with a hybrid machine learning method. Int. J. Appl. Earth Obs. Geoinf. 92, 102174.
Berger, K., Machwitz, M., Kycko, M., Kefauver, S.C., Van Wittenberghe, S., Gerhards, M., Verrelst, J., Atzberger, C., Van Der Tol, C., Damm, A., 2022. Multi-sensor spectral synergies for crop stress detection and monitoring in the optical domain: a review. Remote Sens. Environ. 280, 113198.
Blackburn, G.A., 1998. Spectral indices for estimating photosynthetic pigment concentrations: a test using senescent tree leaves. Int J Remote Sens 19, 657–675.
Bouvet, L., Holdgate, S., James, L., Thomas, J., Mackay, I.J., Cockram, J., 2022. The evolving battle between yellow rust and wheat: implications for global food security. Theoret. Appl. Genet. 1–13.
Breiman, L., 2001. Random forests. Mach. Learn. 45, 5–32.
Calderón, R., Navas-Cortés, J.A., Lucena, C., Zarco-Tejada, P.J., 2013. High-resolution airborne hyperspectral and thermal imagery for early detection of Verticillium wilt of olive using fluorescence, temperature and narrow-band spectral indices. Remote Sens. Environ. 139, 231–245.
Camino, C., Calderón, R., Parnell, S., Dierkes, H., Chemin, Y., Román-Écija, M., Montes-Borrego, M., Landa, B.B., Navas-Cortes, J.A., Zarco-Tejada, P.J., Beck, P.S.A., 2021. Detection of Xylella fastidiosa in almond orchards by synergic use of an epidemic spread model and remotely sensed plant traits. Remote Sens. Environ. 260.
Camino, C., Araño, K., Berni, J.A., Dierkes, H., Trapero-Casas, J.L., León-Ropero, G., Montes-Borrego, M., Roman-Écija, M., Velasco-Amo, M.P., Landa, B.B., 2022. Detecting Xylella fastidiosa in a machine learning framework using Vcmax and leaf biochemistry quantified with airborne hyperspectral imagery. Remote Sens. Environ. 282, 113281.
Chen, X., 2017. Stripe rust epidemiology. Stripe Rust. 283–352.
Chen, X., 2020. Pathogens which threaten food security: Puccinia striiformis, the wheat stripe rust pathogen. Food Security 12, 239–251.
Chen, W., Wellings, C., Chen, X., Kang, Z., Liu, T., 2014. Wheat stripe (yellow) rust caused by P uccinia striiformis f. sp. tritici. Mol. Plant Pathol. 15, 433–446.
Chen, T., Yang, W., Zhang, H., Zhu, B., Zeng, R., Wang, X., Wang, S., Wang, L., Qi, H., Lan, Y., 2020. Early detection of bacterial wilt in peanut plants through leaf-level hyperspectral and unmanned aerial vehicle data. Comput. Electron. Agric. 177, 105708.
Clemente, A.A., Maciel, G.M., Siquieroli, A.C.S., De Araujo Gallis, R.B., Pereira, L.M., Duarte, J.G., 2021. High-throughput phenotyping to detect anthocyanins, chlorophylls, and carotenoids in red lettuce germplasm. Int. J. Appl. Earth Obs. Geoinf. 103, 102533.
Danner, M., Berger, K., Wocher, M., Mauser, W., Hank, T., 2021. Efficient RTM-based training of machine learning regression algorithms to quantify biophysical & biochemical traits of agricultural crops. ISPRS-J. Photogramm. Remote Sens. 173, 278–296.
Daughtry C.S., Walthall C., Kim M., De Colstoun E.B., Mcmurtrey Iii, J., 2000. Estimating corn leaf chlorophyll concentration from leaf and canopy reflectance. Remote Sens. Environ. 74, 229-239.
De Castro, A.I., Ehsani, R., Ploetz, R., Crane, J.H., Abdulridha, J., 2015. Optimum spectral and geometric parameters for early detection of laurel wilt disease in avocado. Remote Sens. Environ. 171, 33–44.
Deng, J., Zhang, X., Yang, Z., Zhou, C., Wang, R., Zhang, K., Lv, X., Yang, L., Wang, Z., Li, P., 2023. Pixel-level regression for UAV hyperspectral images: deep learning-based quantitative inverse of wheat stripe rust disease index. Comput. Electron. Agric. 215, 108434.
Du, K., Jing, X., Zeng, Y., Ye, Q., Li, B., Huang, J., 2023. An improved approach to monitoring wheat stripe rust with sun-induced chlorophyll fluorescence. Remote Sensing 15, 693.
Estévez, J., Salinero-Delgado, M., Berger, K., Pipia, L., Rivera-Caicedo, J.P., Wocher, M., Reyes-Muñoz, P., Tagliabue, G., Boschetti, M., Verrelst, J., 2022. Gaussian processes

retrieval of crop traits in Google Earth Engine based on Sentinel-2 top-of-atmosphere data. Remote Sens. Environ. 273, 112958.
Féret, J.-B., Berger, K., De Boissieu, F., Malenovský, Z., 2021. PROSPECT-PRO for estimating content of nitrogen-containing leaf proteins and other carbon-based constituents. Remote Sens. Environ. 252, 112173.
Fisher, A., Rudin, C., Dominici, F., 2019. All models are wrong, but many are useful: Learning a variable's importance by studying an entire class of prediction models simultaneously. J. Mach. Learn. Res. 20, 1–81.
Gamon, J.A., Huemmrich, K.F., Wong, C.Y., Ensminger, I., Garrity, S., Hollinger, D.Y., Noormets, A., Peñuelas, J., 2016. A remotely sensed pigment index reveals photosynthetic phenology in evergreen conifers. Proc. Natl. Acad. Sci. 113, 13087–13092.
Gamon, J., Penuelas, J., Field, C., 1992. A narrow-waveband spectral index that tracks diurnal changes in photosynthetic efficiency. Remote Sens. Environ. 41, 35–44.
Garrity, S.R., Eitel, J.U., Vierling, L.A., 2011. Disentangling the relationships between plant pigments and the photochemical reflectance index reveals a new approach for remote estimation of carotenoid content. Remote Sens. Environ. 115, 628–635.
Gasmi, A., Gomez, C., Chehbouni, A., Dhiba, D., El Gharous, M., 2022. Using PRISMA hyperspectral satellite imagery and GIS approaches for soil fertility mapping (FertiMap) in northern Morocco. Remote Sens. 14, 4080.
Gitelson A.A., Merzlyak M., Zur Y., Stark R., Gritz U., 2001. Non-destructive and remote sensing techniques for estimation of vegetation status.
Gitelson, A.A., Gritz, Y., Merzlyak, M.N., 2003. Relationships between leaf chlorophyll content and spectral reflectance and algorithms for non-destructive chlorophyll assessment in higher plant leaves. J. Plant Physiol. 160, 271–282.
Gitelson, A.A., Keydan, G.P., Merzlyak, M.N., 2006. Three-band model for noninvasive estimation of chlorophyll, carotenoids, and anthocyanin contents in higher plant leaves. Geophys. Res. Lett. 33.
Gu, Q., Sheng, L., Zhang, T., Lu, Y., Zhang, Z., Zheng, K., Hu, H., Zhou, H., 2019. Early detection of tomato spotted wilt virus infection in tobacco using the hyperspectral imaging technique and machine learning algorithms. Comput. Electron. Agric. 167.
Guo, A., Huang, W., Dong, Y., Ye, H., Ma, H., Liu, B., Wu, W., Ren, Y., Ruan, C., Geng, Y., 2021. Wheat yellow rust detection using UAV-based hyperspectral technology. Remote Sens. 13.
Guo, A., Ye, H., Huang, W., Qian, B., Wang, J., Lan, Y., Wang, S., 2023. Inversion of maize leaf area index from UAV hyperspectral and multispectral imagery. Comput. Electron. Agric. 212, 108020.
Haboudane, D., Miller, J.R., Tremblay, N., Zarco-Tejada, P.J., Dextraze, L., 2002. Integrated narrow-band vegetation indices for prediction of crop chlorophyll content for application to precision agriculture. Remote Sens. Environ. 81, 416–426.
Haboudane, D., Miller, J.R., Pattey, E., Zarco-Tejada, P.J., Strachan, I.B., 2004. Hyperspectral vegetation indices and novel algorithms for predicting green LAI of crop canopies: Modeling and validation in the context of precision agriculture. Remote Sens. Environ. 90, 337–352.
Hearst, M.A., Dumais, S.T., Osuna, E., Platt, J., Scholkopf, B., 1998. Support vector machines. IEEE Intell. Syst. Their. Appl. 13, 18–28.
Hernández-Clemente, R., Navarro-Cerrillo, R.M., Suárez, L., Morales, F., Zarco-Tejada, P. J., 2011. Assessing structural effects on PRI for stress detection in conifer forests. Remote Sens. Environ. 115, 2360–2375.
Hernández-Clemente, R., Hornero, A., Mottus, M., Peñuelas, J., González-Dugo, V., Jiménez, J.C., Suárez, L., Alonso, L., Zarco-Tejada, P.J., 2019. Early diagnosis of vegetation health from high-resolution hyperspectral and thermal imagery: Lessons learned from empirical relationships and radiative transfer modelling. Current Forestry Rep. 5, 169–183.
Liu, W., Chen, Y., Lu, Z., Lu, X., Wu, Z., Zheng, Z., Suo, Y., Lan, C., Yuan, X., 2024. StripeRust-Pocket: a mobile-based deep learning application for efficient disease severity assessment of wheat stripe rust. Plant Phenomics 2024, 0201.
Longmire, A., Poblete, T., Hunt, J., Chen, D., Zarco-Tejada, P., 2022. Assessment of crop traits retrieved from airborne hyperspectral and thermal remote sensing imagery to predict wheat grain protein content. ISPRS-J. Photogramm. Remote Sens. 193, 284–298.
Maimaitijiang, M., Sagan, V., Sidike, P., Maimaitiyiming, M., Hartling, S., Peterson, K.T., Maw, M.J., Shakoor, N., Mockler, T., Fritschi, F.B., 2019. Vegetation index weighted canopy volume model (CVMVI) for soybean biomass estimation from unmanned aerial system-based RGB imagery. ISPRS-J. Photogramm. Remote Sens. [J], 151, 27–41.
Marin D.B., Santana L.S., Barbosa B.D.S., Barata R.a.P., Osco L.P., Ramos A.P.M., Guimarães P.H.S. 2021. Detecting coffee leaf rust with UAV-based vegetation indices and decision tree machine learning models. Comput. Electron. Agric. 190: 106476.
Merzlyak, M.N., Gitelson, A.A., Chivkunova, O.B., Rakitin, V.Y., 1999. Non-destructive optical detection of pigment changes during leaf senescence and fruit ripening. Physiologia Plantarum [j] 106, 135–141.
Moriya É.a.S., Imai N.N., Tommaselli A.M.G., Berveglieri A., Santos G.H., Soares M.A., Marino M., Reis T.T. 2021. Detection and mapping of trees infected with citrus gummosis using UAV hyperspectral data. Comput. Electron. Agric. [J], 188: 106298.
Penuelas, J., Baret, F., Filella, I., 1995. Semi-empirical indices to assess carotenoids/chlorophyll a ratio from leaf spectral reflectance. Photosynthetica [j] 31, 221–230.
Poblete, T., Camino, C., Beck, P., Hornero, A., Kattenborn, T., Saponari, M., Boscia, D., Navas-Cortes, J.A., Zarco-Tejada, P.J., 2020. Detection of Xylella fastidiosa infection symptoms with airborne multispectral and thermal imagery: Assessing bandset reduction performance from hyperspectral analysis. ISPRS-J. Photogramm. Remote Sens. 162, 27–40.
Poblete, T., Navas-Cortes, J., Camino, C., Calderon, R., Hornero, A., Gonzalez-Dugo, V., Landa, B., Zarco-Tejada, P., 2021. Discriminating Xylella fastidiosa from Verticillium dahliae infections in olive trees using thermal-and hyperspectral-based plant traits. ISPRS-J. Photogramm. Remote Sens. 179, 133–144.
Poblete, T., Navas-Cortes, J.A., Hornero, A., Camino, C., Calderon, R., Hernandez-Clemente, R., Landa, B., Zarco-Tejada, P.J., 2023. Detection of symptoms induced by vascular plant pathogens in tree crops using high-resolution satellite data: Modelling and assessment with airborne hyperspectral imagery. Remote Sens. Environ. 295, 113698.
Rumpf, T., Mahlein, A.-K., Steiner, U., Oerke, E.-C., Dehne, H.-W., Plümer, L., 2010. Early detection and classification of plant diseases with support vector machines based on hyperspectral reflectance. Comput. Electron. Agric. 74, 91–99.
Shahi, T.B., Xu C.-Y., Neupane, A., Guo, W., 2023. Recent advances in crop disease detection using UAV and deep learning techniques. Remote Sens. [J], 15: 2450.
Shi, Y., Huang, W., González-Moreno, P., Luke, B., Dong, Y., Zheng, Q., Ma, H., Liu, L., 2018. Wavelet-based rust spectral feature set (WRSFs): a novel spectral feature set based on continuous wavelet transformation for tracking progressive Host–Pathogen interaction of yellow rust on wheat. Remote Sens. 10.
Snoek J., Larochelle H., Adams, R.P., 2012. Practical bayesian optimization of machine learning algorithms. Advances in neural information processing systems [J], 25.
Suarez, L., González-Dugo, V., Camino, C., Hornero, A., Zarco-Tejada, P.J., 2021. Physical model inversion of the green spectral region to track assimilation rate in almond trees with an airborne nano-hyperspectral imager. Remote Sens. Environ. 252, 112147.
Tang, Z., Wang, M., Schirrmann, M., Dammer, K.-H., Li, X., Brueggeman, R., Sankaran, S., Carter, A.H., Pumphrey, M.O., Hu, Y., 2023. Affordable high throughput field detection of wheat stripe rust using deep learning with semi-automated image labeling. Comput. Electron. Agric. 207, 107709.
Tasci, B., Acharya, M.R., Baygin, M., Dogan, S., Tuncer, T., Belhaouari, S.B., 2023. InCR: Inception and concatenation residual block-based deep learning network for damaged building detection using remote sensing images. Int. J. Appl. Earth Obs. Geoinf. 123, 103483.
Tian, L., Xue, B., Wang, Z., Li, D., Yao, X., Cao, Q., Zhu, Y., Cao, W., Cheng, T., 2021. Spectroscopic detection of rice leaf blast infection from asymptomatic to mild stages with integrated machine learning and feature selection. Remote Sens. Environ. 257, 112350.
Tian, L., Wang, Z., Xue, B., Li, D., Zheng, H., Yao, X., Zhu, Y., Cao, W., Cheng, T., 2023. A disease-specific spectral index tracks Magnaporthe oryzae infection in paddy rice from ground to space. Remote Sens. Environ. 285, 113384.
Trifi, M., Gasmi, A., Carbone, C., Majzlan, J., Nasri, N., Dermech, M., Charef, A., Elfil, H., 2022. Machine learning-based prediction of toxic metals concentration in an acid mine drainage environment, northern Tunisia. Environ. Sci. Pollution Res. 29, 87490–87508.
Verrelst, J., Rivera, J.P., Veroustraete, F., Muñoz-Marí, J., Clevers, J.G., Camps-Valls, G., Moreno, J., 2015. Experimental Sentinel-2 LAI estimation using parametric, non-parametric and physical retrieval methods – a comparison. ISPRS-J. Photogramm. Remote Sens. 108, 260–272.
Vogelmann, J., Rock, B., Moss, D., 1993. Red edge spectral measurements from sugar maple leaves. Remote Sens 14, 1563–1575.
Watt, M.S., Poblete, T., De Silva, D., Estarija, H.J.C., Hartley, R.J., Leonardo, E.M.C., Massam, P., Buddenbaum, H., Zarco-Tejada, P.J., 2023. Prediction of the severity of Dothistroma needle blight in radiata pine using plant based traits and narrow band indices derived from UAV hyperspectral imagery. Agric. For. Meteorol. 330, 109294.
Wei, P., Lu, Z., Song, J., 2015. Variable importance analysis: a comprehensive review. Reliab Eng Syst Saf 142, 399–432.
Wu, G., Fang, Y., Jiang, Q., Cui, M., Li, N., Ou, Y., Diao, Z., Zhang, B., 2023. Early identification of strawberry leaves disease utilizing hyperspectral imaging combing with spectral features, multiple vegetation indices and textural features. Comput Electron Agric 204, 107553.
Wu, L., Wang, L., Shi, C., Yin, D., 2022. Detecting mangrove photosynthesis with solar-induced chlorophyll fluorescence. Int J Remote Sens 43, 1037–1053.
Wu, L., Zhang, Y., Zhang, Z., Zhang, X., Wu, Y., Chen, J.M., 2024. Deriving photosystem-level red chlorophyll fluorescence emission by combining leaf chlorophyll content and canopy far-red solar-induced fluorescence: possibilities and challenges. Remote Sens. Environ. 304, 114043.
Yao, Z., Lei, Y., He, D., 2019. Early visual detection of wheat stripe rust using visible/near-infrared hyperspectral imaging. Sensors 19.
Zarco-Tejada, P.J., Camino, C., Beck, P.S.A., Calderon, R., Hornero, A., Hernández-Clemente, R., Kattenborn, T., Montes-Borrego, M., Susca, L., Morelli, M., Gonzalez-Dugo, V., North, P.R.J., Landa, B.B., Boscia, D., Saponari, M., Navas-Cortes, J.A., 2018. Previsual symptoms of Xylella fastidiosa infection revealed in spectral plant-trait alterations. Nat. Plants 4, 432–439.
Zarco-Tejada, P., Poblete, T., Camino, C., Gonzalez-Dugo, V., Calderon, R., Hornero, A., Hernandez-Clemente, R., Román-Écija, M., Velasco-Amo, M., Landa, B., 2021. Divergent abiotic spectral pathways unravel pathogen stress signals across species. Nat. Commun. 12, 1–11.
Zhang, J., Jing, X., Song, X., Zhang, T., Duan, W., Su, J., 2023. Hyperspectral estimation of wheat stripe rust using fractional order differential equations and Gaussian process methods. Comput Electron Agric 206, 107671.
Zheng, Q., Huang, W., Cui, X., Shi, Y., Liu, L., 2018. New spectral index for detecting wheat yellow rust using Sentinel-2 multispectral imagery. Sensors [j] 18.
Zhu, W., Sun, Z., Yang, T., Li, J., Peng, J., Zhu, K., Li, S., Gong, H., Lyu, Y., Li, B., 2020. Estimating leaf chlorophyll content of crops via optimal unmanned aerial vehicle hyperspectral data at multi-scales. Comput. Electron. Agric. [J], 178, 105786.